J. Fluid Mech. (1989), *vol.* 209, *pp.* 265–284
Printed in Great Britain

Nonlinear Faraday resonance in a box with a square base

By M. NAGATA

Department of Mathematical Sciences, University of St Andrews, North Haugh, St Andrews KY16 9SS, Fife, UK

(Received 6 December 1988)

Surface wave motions in a container with a square base, which is subject to a vertical oscillation, are considered when the amplitude of the oscillation is small and the frequency of the oscillation is close to twice the natural frequency of the system. Subcritical wave motions are found for single modes as well as mixed modes. Here, single modes are described by either one of the two horizontal coordinates whereas mixed modes depend on both coordinates. It is found that in some subcritical region a stable single mode and a stable mixed mode coexist, producing complex basins of attraction.

1. Introduction

In an experiment on surface wave in a vertically oscillating container, Faraday (1831) noticed that the frequency of surface waves was one half the frequency of the forcing oscillation. More than half a century after the further investigations on this matter by Rayleigh (1883*a*, *b*), Benjamin & Ursell (1954) explained this subharmonic excitation of the surface waves by analysing an infinite set of Mathieu's equations derived from the linear theory of irrotational motion of an ideal fluid. This classical problem of hydrodynamic instability has recently arisen again in two rather different ways. One of these concerns the sometimes chaotic behaviour observed in a container with a closed basin (Keolian *et al.* 1981; Gollub & Meyer 1983; Ciliberto & Gollub 1984, 1985; Holmes 1986; Simonelli & Gollub 1989). The other relates to solitary standing waves observed in a long narrow channel (Wu, Keolian & Rudnick 1984; Larraza & Putterman 1984; Miles 1984*b*).

In this paper, we consider the case where the container has a square base in order to examine competition between a single wave mode and a mixed wave mode, both of which have the same critical point. The analysis was inspired by the planform selection problem in thermal convection (Swift 1984; Jenkins 1987). Mathieu's equation in conjunction with the Faraday resonance is

$$\frac{\mathrm{d}^2A}{\mathrm{d}t^2}+(g-f\cos 2\omega t)\frac{\pi}{l}\tanh\left(\frac{\pi}{l}h\right)A=0, \tag{1.1}$$

where g is the acceleration due to gravity, and f and 2ω are the amplitude and the frequency of the forcing oscillation, respectively (Drazin & Reid 1981, p. 357). Since l, the side length of the square basin, and h, the height of the fluid relative to the basin, are fixed in our configuration of the problem, the system determines the natural frequency

$$\omega_0=\left[\frac{\pi}{l}g\tanh\left(\frac{\pi}{l}h\right)\right]^{\frac{1}{2}}, \tag{1.2}$$

which corresponds to the free oscillation of surface waves at $f = 0$. These are the lowest frequency side-to-side 'sloshing modes' with just half a wavelength between the sidewalls. When the forcing frequency 2ω is tuned in such a way that $\omega = \omega_0$, surface waves with a frequency ω_0 become marginally stable at $f = 0$ in inviscid fluid. If the forcing frequency is slightly off-tuned, the onset of the surface waves with frequency ω_0 in the linear theory is delayed until some finite f. We concentrate our attention on the case where f and $|\omega^2 - \omega_0^2|$ are small in the same order, and perform a weakly nonlinear analysis. In the process, a weak damping attributable to viscous effects is incorporated. Our approach to the problem of Faraday resonance is different from Miles' (1984*a*). He uses a Lagrangian and Hamiltonian formulation, whereas the classical expansion procedure and the multiple timescale analysis is performed in our approach. Although our analysis is tedious, it clearly interprets the bifurcation sequence of Miles as the supercritical and the subcritical bifurcations of the surface waves depending on ω when it is fixed. Moreover, the resonance of two single wave modes is easily formulated in our analysis in contrast to the complication which prevented Miles from obtaining explicit results.

More recently, Feng & Sethna (1989) considered surface wave motions in a container with a nearly square base subjected to a vertical oscillation. They employed perturbation expansions, as here. Their treatment is more general in that they consider rectangular 'nearly square' containers; but their emphasis is on the symmetry-breaking aspect of the problem rather than classification of bifurcation sequences which occur when the symmetry is preserved. They choose just one example in a parameter range which covers the case of infinite fluid depth. As will be made clear later, there are, in fact, five different parameter ranges determined by the configuration of the problem even in the exactly square case. Basically their results were obtained numerically. In the present paper the absence of the symmetry-breaking factor allows us to obtain explicit expressions analytically for the stability of the single mode (§3.2) and the mixed mode (§3.3.3) and for the general mode solution (§3.3.2). The classification of the bifurcation diagram becomes possible only when such explicit expressions are obtained. The stability of the flat surface (§3.1) and the descriptions of the single mode solutions (§3.2) and the mixed mode solutions (§3.3.3) are not novel but necessary for the analysis. We provide a numerical example in §4 in order to examine a situation where multiple stable solutions coexist. The formulation of the problem is described in §2 and the results are summarized in the last section.

2. Description of the problem

We consider irrotational surface wave motions of an ideal fluid layer with a depth h in a rectangular container, which has a square base with side length l and is subject to an oscillatory vertical acceleration $f\cos 2\omega t$ (see figure 1). The fluid motion is described by a velocity potential $\Phi(x, y, z, t)$ which satisfies Laplace's equation

$$\nabla^2\Phi = 0 \quad \text{in} \quad -h < x < \zeta, \tag{2.1}$$

where $z = \zeta(x, y, t)$ is the elevation of the fluid surface. The bottom and the side boundary conditions are

$$\frac{\partial\Phi}{\partial z} = 0: \quad z = -h, \quad \frac{\partial\Phi}{\partial x} = 0: \quad x = 0, l, \quad \frac{\partial\Phi}{\partial y} = 0: \quad y = 0, l. \tag{2.2a,b,c}$$

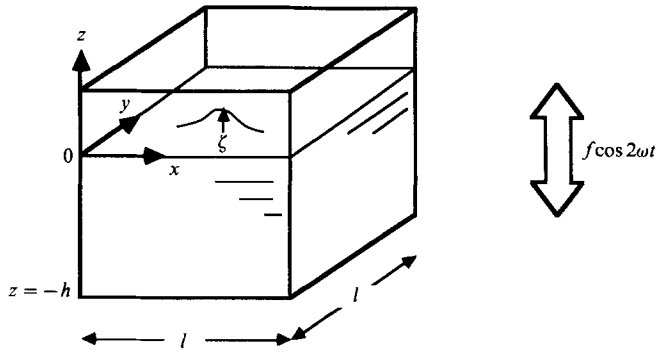

FIGURE 1. Configuration of the problem.

On the surface $z = \zeta$, the kinematic and pressure conditions

$$\frac{\partial \zeta}{\partial t}+\frac{\partial \Phi}{\partial x}\frac{\partial \zeta}{\partial x}+\frac{\partial \Phi}{\partial y}\frac{\partial \zeta}{\partial y}=\frac{\partial \Phi}{\partial z}, \tag{2.3a}$$

$$\frac{\partial \Phi}{\partial t}+(g-f\cos 2\omega t)\,\zeta=\tfrac{1}{2}(\nabla\Phi)^2 \tag{2.3b}$$

are applied, where g is the gravitational acceleration. Surface tension is neglected but its incorporation would not present major difficulties.

We assume that for a small parameter ϵ,

$$f\sim O(\epsilon^2), \quad \Phi,\zeta\sim O(\epsilon)$$

so that after expansion in ζ about $z = 0$, (2.3a) and (2.3b) are combined to give a nonlinear condition for Φ,

$$\begin{aligned}\frac{\partial^2\Phi}{\partial t^2}+g\frac{\partial\Phi}{\partial z}=&-\left\{\frac{\partial}{\partial t}(\nabla\Phi)^2-\frac{\partial}{\partial z}\left[\left(\frac{\partial\Phi}{\partial z}+\frac{1}{g}\frac{\partial^2\Phi}{\partial t^2}\right)\frac{\partial\Phi}{\partial t}\right]\right\}\\&-\frac{1}{2}\left\{\frac{\partial}{\partial x}(\nabla\Phi)^2\frac{\partial\Phi}{\partial x}+\frac{\partial}{\partial y}(\nabla\Phi)^2\frac{\partial\Phi}{\partial y}+\frac{\partial}{\partial z}(\nabla\Phi)^2\frac{\partial\Phi}{\partial z}-\frac{2}{g}\frac{\partial}{\partial z}\left[\frac{\partial}{\partial t}(\nabla\Phi)^2\frac{\partial\Phi}{\partial t}\right]\right.\\&\left.-\left[(\nabla\Phi)^2-\frac{2}{g}\frac{\partial}{\partial z}\left(\frac{\partial\Phi}{\partial t}\right)^2\right]\frac{\partial}{\partial z}\left(\frac{\partial\Phi}{\partial z}+\frac{1}{g}\frac{\partial^2\Phi}{\partial t^2}\right)\right\}\\&+f\left(\cos 2\omega t\frac{\partial\Phi}{\partial z}+\frac{2\omega}{g}\sin 2\omega t\frac{\partial\Phi}{\partial t}\right)\quad\text{at}\quad z=0,\end{aligned} \tag{2.4}$$

which is valid up to the cubic order in ϵ; cf. Larraza & Putterman (1984). Then, Laplace's equation (2.1) is to be solved in $-h < z < 0$ with the boundary conditions (2.2a, b, c) and (2.4).

We expect a surface wave motion with a frequency $\omega(=2\omega/2)$ and assume that

$$|\omega^2-\omega_0^2|\sim O(\epsilon^2),$$

where

$$\omega_0=[\alpha g\tanh(\alpha h)]^{\frac{1}{2}} \tag{2.5}$$

is the natural frequency of the system with a wavenumber

$$\alpha=\frac{\pi}{l}. \tag{2.6}$$

It is convenient to introduce a long timescale T and replace $\partial/\partial t$ in (2.4) by $\partial/\partial t+\epsilon^2\partial/\partial T$. Also, we expand ϕ in powers of the small parameter ϵ as

$$\Phi = \epsilon\phi^{(1)}+\epsilon^2\phi^{(2)}+\dots. \tag{2.7}$$

At leading order in ϵ, the linear equation for the gravity wave

$$\frac{\partial^2\phi^{(1)}}{\partial t^2}+g\frac{\partial\phi^{(1)}}{\partial z}=0 \quad \text{at} \quad z=0 \tag{2.8}$$

is recovered. The solution of Laplace's equation with the boundary conditions (2.2a, b, c) and (2.8) is

$$\phi^{(1)} = A(T)\cos\alpha x\,\mathrm{e}^{\mathrm{i}\omega t}\frac{\cosh\{\alpha(z+h)\}}{\cosh(\alpha h)}+B(T)\cos\alpha y\,\mathrm{e}^{\mathrm{i}\omega t}\frac{\cosh\{\alpha(z+h)\}}{\cosh(\alpha h)}+\text{c.c.} \tag{2.9}$$

Note that the discrepancy from zero when (2.9) is substituted into (2.8) is

$$(\omega_0^2-\omega^2)\left[A(T)\cos\alpha x\,\mathrm{e}^{\mathrm{i}\omega t}\frac{\cosh\{\alpha(z+h)\}}{\cosh(\alpha h)}+B(T)\cos\alpha y\,\mathrm{e}^{\mathrm{i}\omega t}\frac{\cosh\{\alpha(z+h)\}}{\cosh(\alpha h)}+\text{c.c.}\right]$$

and will be taken care of later in the equation for the cubic order in ϵ.

The evolution of a single surface wave mode, either $A\neq 0$, $B=0$ or $A=0$, $B\neq 0$, and a mixed surface wave mode $A\neq 0$, $B\neq 0$ on a long timescale T is our concern.

At second order in the expansion, the boundary condition (2.4) becomes

$$\frac{\partial^2\phi^{(2)}}{\partial t^2}+g\frac{\partial\phi^{(2)}}{\partial z}=-\frac{\partial}{\partial t}(\nabla\phi^{(1)}\,\nabla\phi^{(1)})+\frac{\partial}{\partial z}\left[\left(\frac{\partial\phi^{(1)}}{\partial z}+\frac{1}{g}\frac{\partial^2\phi^{(1)}}{\partial t^2}\right)\frac{\partial\phi^{(1)}}{\partial t}\right] \quad \text{at} \quad z=0. \tag{2.10}$$

The appropriate solution of Laplace's equation with the boundary conditions (2.2a, b, c) and (2.10) is given by

$$\begin{aligned}\phi^{(2)} = {} & C(T)\cos 2\alpha x\,\mathrm{e}^{2\mathrm{i}\omega t}\frac{\cosh\{2\alpha(z+h)\}}{\cosh(2\alpha h)}+D(T)\,\mathrm{e}^{2\mathrm{i}\omega t}\\ & +E(T)\cos 2\alpha y\,\mathrm{e}^{2\mathrm{i}\omega t}\frac{\cosh\{2\alpha(z+h)\}}{\cosh(2\alpha h)}+H(T)\cos\alpha x\cos\alpha y\,\mathrm{e}^{2\mathrm{i}\omega t}\frac{\cosh\{\sqrt{2}\alpha(z+h)\}}{\cosh(\sqrt{2}\alpha h)}\\ & +L(T)\cos\alpha x\,\mathrm{e}^{\mathrm{i}\omega t}\frac{\cosh\{\alpha(z+h)\}}{\cosh(\alpha h)}+M(T)\cos\alpha y\,\mathrm{e}^{\mathrm{i}\omega t}\frac{\cosh\{\alpha(z+h)\}}{\cosh(\alpha h)}\\ & +J(T)\,t+\text{c.c.},\end{aligned} \tag{2.11}$$

where

$$C(T) = -\frac{3\mathrm{i}\alpha^2(1+\sigma^2)(1-\sigma^2)}{8\omega\sigma^2}A^2, \qquad D(T)=\frac{\mathrm{i}\alpha^2(3\sigma^2+1)}{8\omega}(A^2+B^2), \tag{2.12a, b}$$

$$E(T) = -\frac{3\mathrm{i}\alpha^2(1+\sigma^2)(1-\sigma^2)}{8\omega\sigma^2}B^2, \qquad H(T)=\frac{2\mathrm{i}\alpha^2(3\sigma^2-1)\sigma}{\omega(4\sigma-\sqrt{2}\tilde{\sigma})}AB, \tag{2.12c, d}$$

$$J(T) = -\tfrac{1}{2}\alpha^2(1-\sigma^2)(|A|^2+|B|^2), \tag{2.12e}$$

with

$$\sigma=\tanh(\alpha h), \quad \tilde{\sigma}=\tanh(\sqrt{2}\alpha h). \tag{2.13a, b}$$

It will turn out that $L(T)$ and $M(T)$ do not play a role in the following analysis. Conservation of mass requires $J(T)$.

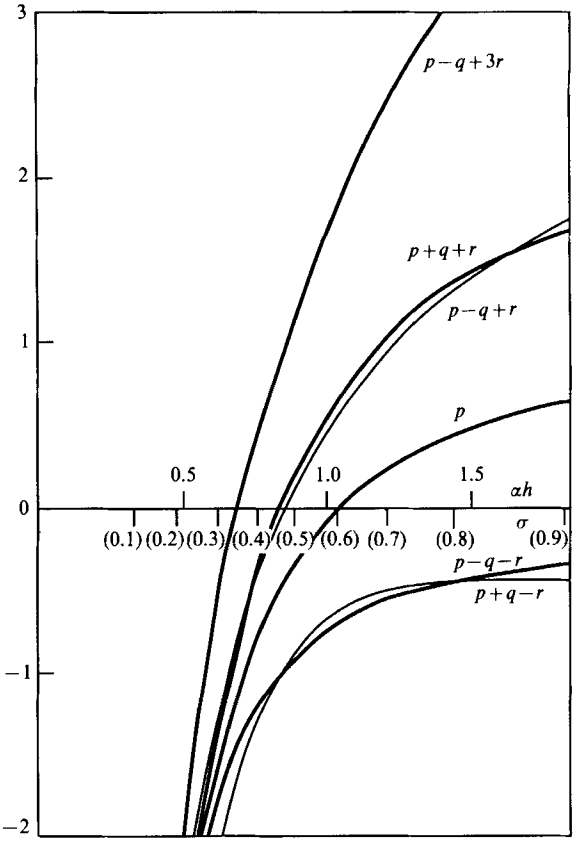

FIGURE 2. p and other combinations of p, q and r as a function of αh or $\sigma = \tanh(\alpha h)$. Graphs are normalized by $2\omega_0 \alpha^{-4}$.

At third order in ϵ, the following set of evolution equations is obtained:

$$\mathrm{i}\left(\frac{\partial}{\partial T}+\mu\right)A = \Omega A + FA^* + (p|A|^2+q|B|^2)A + rB^2A^*, \tag{2.14a}$$

$$\mathrm{i}\left(\frac{\partial}{\partial T}+\mu\right)B = \Omega B + FB^* + (q|A|^2+p|B|^2)B + rA^2B^*, \tag{2.14b}$$

where

$$\Omega = \frac{(\omega^2-\omega_0^2)}{2\omega_0\epsilon^2}, \quad F = -\frac{f\omega_0}{4g\epsilon^2} \tag{2.15a, b}$$

and

$$p = \frac{\alpha^4(-9\sigma^{-2}+12+3\sigma^2+2\sigma^4)}{16\omega_0}, \tag{2.16a}$$

$$q = \frac{\alpha^4\{2\sigma(3\sigma^2-1)^2/(\sqrt{2\tilde{\sigma}}-4\sigma)-2\sigma^2+5\sigma^4\}}{2\omega_0}, \quad r = \frac{\alpha^4(2+\sigma^2)\sigma^2}{4\omega_0}. \tag{2.16b, c}$$

In the evolution equations above, an asterisk denotes complex conjugation, and weak linear damping $\epsilon^2\mu$ (> 0) is incorporated following Miles (1984*a*). Separation of A into real and imaginary parts in (2.14*a*) leads to the same type of evolution

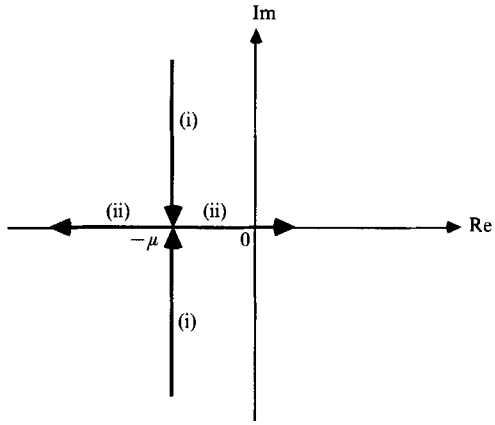

FIGURE 3. The trace of the eigenvalue associated with the stability of the flat surface on the complex plane when F^2 is increased.

equations as Miles' (1984*b*, see his equation (5.2*a*, *b*)) when $B \equiv 0$. The set of evolution equations (2.14*a*, *b*) is identical to the one obtained by Feng & Sethna (1989).

In figure 2, p together with some combinations of p, q and r which will be needed in the later analysis, is plotted as a function of αh.

3. Analysis

3.1. *Stability of the flat surface*

Linear stability analysis for the origin $A = B = 0$ is straightforward. The real part $\tilde{A}_R$ and imaginary part $\tilde{A}_I$ of an infinitesimal perturbation $\tilde{A}$ (or $\tilde{B}$) satisfy

$$\frac{\partial}{\partial T}\begin{pmatrix}\tilde{A}_R\\ \tilde{A}_I\end{pmatrix} = \begin{pmatrix}-\mu & \Omega - F\\ -\Omega - F & -\mu\end{pmatrix}\begin{pmatrix}\tilde{A}_R\\ \tilde{A}_I\end{pmatrix}. \tag{3.1}$$

The eigenvalue λ is obtained by

$$(\lambda+\mu)^2 = F^2 - \Omega^2. \tag{3.2}$$

Hence, when $F^2 \geqslant \Omega^2$

$$\lambda = -\mu \pm (F^2 - \Omega^2)^{\frac{1}{2}} \tag{3.3a}$$

and when $F^2 < Q^2$,

$$\lambda = -\mu \pm \mathrm{i}(-F^2 + \Omega^2)^{\frac{1}{2}}. \tag{3.3b}$$

We find that the origin becomes unstable (saddle) when $F^2 > \Omega^2 + \mu^2$. When the origin is stable, the eigenvalues are either (i) complex with real part $-\mu$ for $0 < F^2 < \Omega^2$ or (ii) they take two negative real values for $Q^2 < F^2 < \Omega^2 + \mu^2$ (see figure 3).

3.2. *Single surface wave motion*

By setting $\partial/\partial T \equiv 0$ in (2.14*a*), i.e.

$$\mathrm{i}\mu A_0 = \Omega A_0 + F A_0^* + p|A_0|^2 A_0 \tag{3.4}$$

we can obtain the single surface wave motion

$$A = A_0 \equiv a_0 \mathrm{e}^{\mathrm{i}\theta} \neq 0, \quad B = 0$$

where
$$a_0 = \left[\frac{-\Omega \pm (F^2-\mu^2)^{\frac{1}{2}}}{p}\right]^{\frac{1}{2}} \tag{3.5a}$$

and
$$\sin 2\theta = \mu/F < 0. \tag{3.5b}$$

Alternative signs appearing subsequently in this subsection are consistent with that in (3.5*a*). By symmetry the other single surface wave solution $B = B_0 \neq 0, A = 0$ has identical properties. The alternative signs for a_0 in (3.5*a*) correspond to whether $\cos 2\theta$ is positive or negative; they do not imply that there are always two possible a_0 values, for a_0^2 cannot be negative. From (3.5*b*) we find that there are two possible single surface wave motions for each positive a_0 with $B = 0$, whose phases are different by π. It turns out that only one of the alternative a_0 values is possible for $p > 0, \Omega > 0$ or $p < 0, \Omega < 0$ when F^2 exceeds the critical value $\Omega^2+\mu^2$ (supercritical bifurcation), and that both a_0 values are present for $p > 0, \Omega < 0$ or $p < 0, \Omega > 0$ when $\mu^2 < F^2 < \Omega^2+\mu^2$ (subcritical bifurcation). Meron (1987) has already examined the subcritical bifurcation of single surface wave motions through their evolution equation which was derived only by summetry considerations. A few years earlier than Meron (1987), Miles (1984*a*) seemed to realize this subcriticality as he noticed an energy jump in some parameter region (see his figure 3).

In order to analyse the stability of the single surface wave solution, perturbations $\tilde{A}$ and $\tilde{B}$ are superimposed on $A = A_0$ and $B = 0$, respectively. Retaining only terms which are linear in $\tilde{A}$ and $\tilde{B}$ (and their complex conjugates), we get

$$\frac{\partial \tilde{A}}{\partial T} = -\mu\tilde{A} - \mathrm{i}\Omega\tilde{A} - \mathrm{i}F\tilde{A}^* - \mathrm{i}p(A_0^2\tilde{A}^* + 2|A_0|^2\tilde{A}), \tag{3.6a}$$

$$\frac{\partial \tilde{B}}{\partial T} = -\mu\tilde{B} - \mathrm{i}\Omega\tilde{B} - \mathrm{i}F\tilde{B}^* - \mathrm{i}q|A_0|^2\tilde{B} - \mathrm{i}rA_0^2\tilde{B}^*, \tag{3.6b}$$

with A_0 as defined above. The perturbations $\tilde{A}$ and $\tilde{B}$ do not interact with each other.

Let us examine (3.6*a*) first, which after some manipulation yields the equation for the eigenvalue λ
$$(\lambda+\mu)^2 = -4\{F^2 - \tfrac{5}{4}\mu^2 \pm \Omega(F^2-\mu^2)^{\frac{1}{2}}\}. \tag{3.7}$$

The sum of the two eigenvalues is -2μ.

In the following, we shall consider the case where $p < 0$ for fixed Ω. When $p > 0$, the treatment is similar.

For the supercritical solution
$$a_0 = \left[\frac{-\Omega - (F^2-\mu^2)^{\frac{1}{2}}}{p}\right]^{\frac{1}{2}} \tag{3.8}$$

with $\Omega < 0$, the eigenvalue satisfies
$$(\lambda+\mu)^2 = 4\{-\Omega^2[1+s-(1+s)^{\frac{1}{2}}] + \tfrac{1}{4}\mu^2\}, \tag{3.9}$$

where $s \geqslant 0$ is defined in such a way that
$$F^2 = \Omega^2(1+s) + \mu^2. \tag{3.10}$$

Since $1+s \geqslant (1+s)^{\frac{1}{2}}$ for $s \geqslant 0$, we get $(\lambda+\mu)^2 \leqslant \mu^2$. Hence, real parts of both eigenvalues are negative.

For the subcritical solution with $\Omega > 0$, the upper solution branch is given by
$$a_0 = \left[\frac{-\Omega - (F^2-\mu^2)^{\frac{1}{2}}}{p}\right]^{\frac{1}{2}}, \tag{3.11}$$

whereas the lower solution branch is given by

$$a_0 = \left[\frac{-\Omega + (F^2-\mu^2)^{\frac{1}{2}}}{p}\right]^{\frac{1}{2}}. \tag{3.12}$$

Correspondingly, the eigenvalue λ satisfies

$$(\lambda+\mu)^2 = 4\{-(S_u^{\frac{1}{2}}+S_u)\,\Omega^2+\tfrac{1}{4}\mu^2\}, \tag{3.13}$$

where $S_u \geqslant 0$ is defined as

$$S_u = (F^2-\mu^2)/\Omega^2 \tag{3.14}$$

for the upper solution branch, and λ satisfies

$$(\lambda+\mu)^2 = 4\{(S_l^{\frac{1}{2}}-S_l)\,\Omega^2+\tfrac{1}{4}\mu^2\} \tag{3.15}$$

for the lower solution branch where S_l is defined by a similar way as S_u, namely

$$S_l = (F^2-\mu^2)/\Omega^2 \tag{3.16}$$

but $0 \leqslant S_l \leqslant 1$.

It can be seen that real parts of the two eigenvalues are both negative on the upper solution branch, whereas one of the two eigenvalues becomes positive on the lower solution branch, changing the sign at the turning point $F^2 = \mu^2$ or $S_u = S_l = 0$. So far the stability properties with respect to perturbation $\tilde{A}$ are quite normal; namely the supercritical solutions are stable whereas the subcritical solutions on the lower branch are unstable and gain stability at the turning point. However, stability must also be examined with respect to perturbations $\tilde{B}$. For (3.6*b*), the eigenvalue λ satisfies

$$(\lambda+\mu)^2 = \left(1-\frac{2r}{p}+\frac{r^2-q^2}{p^2}\right)F^2+\left(-1+\frac{2q}{p}+\frac{r^2-q^2}{p^2}\right)\Omega^2$$
$$+\left(\frac{2r}{p}-\frac{r^2-q^2}{p^2}\right)\mu^2 \pm 2\left(\frac{r}{p}-\frac{q}{p}-\frac{r^2-q^2}{p^2}\right)Q(F^2-\mu^2)^{\frac{1}{2}}. \tag{3.17}$$

For the supercritical solution, (3.17) yields

$$(\lambda+\mu)^2 = \mu^2+\hat{f}(s)\,\Omega^2, \tag{3.18}$$

where s is defined by (3.10) and

$$\hat{f}(s) = P+Qs+P(1+s)^{\frac{1}{2}}\frac{|\Omega|}{\Omega}, \tag{3.19}$$

with

$$P = 2\left(-\frac{r}{p}+\frac{q}{p}+\frac{r^2-q^2}{p^2}\right), \quad Q = 1-\frac{2r}{p}+\frac{r^2-q^2}{p^2}. \tag{3.20a, b}$$

When p is positive (hence $|\Omega| = \Omega$), $\hat{f}(s)$ is given by

$$\hat{f}(s) = P+Qs-P(1+s)^{\frac{1}{2}}.$$

Obviously, $\hat{f}(0) = 0$, and $s = s_1 = P(P-2Q)/Q^2$ satisfies $\hat{f} = 0$ only when $(P-Q)/Q > 0$, i.e. $(p-q+r)/(p+q-r) < 0$. It is found that for $0 < s \ll 1$,

$$\hat{f} \approx P+Qs-P(1+\tfrac{1}{2}s) = \frac{p-q-r}{p}s < 0$$

because $p-q-r<0$ (see figure 2). Therefore, the only case where $\hat{f}$ is positive is when $p-q+r>0$ and $p+q-r<0$, and for

$$F^2>\mu^2+(1+s_1)\Omega^2=\mu^2+\frac{(p-q+r)^2}{(p+q-r)^2}\Omega^2\equiv R_1$$

(when $p-q+r<0$ and $p+q-r>0$, s_1 is negative so that $\hat{f}$ is negative for $F^2>\mu^2+\Omega^2$).

When p is negative (hence $|\Omega|=-\Omega$), $\hat{f}(s)$ is again given by (3.21). The same argument as above, except that $\hat{f}>0$ for $0<s\ll 1$, leads to the conclusion that $\hat{f}$ is negative only when $p-q+r<0$ and $p+q-r>0$ and for $F^2>R_1$. However, this condition cannot be met as figure 2 indicates. Thus, the supercritical single mode is always unstable when $p<0$.

The stability of the subcritical solutions with respect to perturbations $\tilde{B}$ is dealt with similarly. When $p-q+r>0$ and $p+q-r>0$, the lower branch is unstable and the upper branch is stable for $F^2>R_1$, irrespective of the sign of p. When $p-q+r<0$ and $p+q-r<0$, the lower branch is stable and the upper branch is unstable for $F^2>R_1$, again irrespective of the sign of p. When $p-q+r>0$ and $p+q-r<0$, stability occurs only when $p<0$ and $R_1<F^2<\mu^2+\Omega^2$. When $p-q+r<0$ and $p+q-r>0$, instability occurs only when $p>0$ and $R_1<F^2<\mu^2+\Omega^2$. Since $p+q-r<0$ always (see figure 2), many possibilities are eliminated. In order to get overall stability, the normal stability properties derived from (3.6*a*) must also be taken into account.

3.3. *Double surface wave motion*

The set of evolution equations (2.14*a*, *b*) has double mode solutions, $A=a\,\mathrm{e}^{\mathrm{i}\phi}$, $B=b\mathrm{e}^{\mathrm{i}\psi}$ with $ab\neq 0$. After setting $\partial/\partial T\equiv 0$, real and imaginary parts of the equations are separated into

$$\Omega+F\cos 2\phi+pa^2+qb^2+rb^2\cos 2(\phi-\psi)=0, \tag{3.22a}$$

$$\Omega+F\cos 2\psi+qa^2+pb^2+ra^2\cos 2(\phi-\psi)=0, \tag{3.22b}$$

$$\mu+F\sin 2\phi+rb^2\sin 2(\phi-\psi)=0, \tag{3.22c}$$

$$\mu+F\sin 2\psi-ra^2\sin 2(\phi-\psi)=0. \tag{3.22d}$$

3.3.1. *Case when sin* $2(\phi-\psi)=0$: *mixed mode*

When $\sin 2(\phi-\psi)=0$, i.e. $\phi-\psi=\frac{1}{2}n\pi$ (n integer), (3.22*c*, *d*) give

$$\sin 2\phi=\sin 2\psi \tag{3.23a}$$

because $F\neq 0$. Therefore, n must be an even integer, that is, the phases of A and B are the same or different by π. In this case,

$$\cos 2(\phi-\psi)=1 \quad\text{and}\quad \cos 2\phi=\cos 2\psi. \tag{3.23b, c}$$

Subtracting (3.22*b*) from (3.22*a*), we get

$$(p-q-r)(a^2-b^2)=0 \tag{3.24}$$

by using (3.23*b*, *c*). Since $p-q-r<0$ (see figure 2), two amplitudes a and b are equal:

$$a=b. \tag{3.25}$$

Then, the following set of equations is obtained:

$$\Omega+F\cos 2\phi+(p+q+r)a^2=0, \quad \mu+F\sin 2\phi=0.$$

Comparison of these equations with (3.4) for the single surface wave motion leads to

$$a = b = \left[\frac{-\Omega \pm (F^2-\mu^2)^{\frac{1}{2}}}{p+q+r}\right]^{\frac{1}{2}}, \tag{3.26a}$$

$$\sin 2\phi = \sin 2\psi = \mu/F < 0. \tag{3.26b}$$

We call this solution the mixed mode. This mode is characterized by the corner-to-corner surface wave. It is immediately found that the mixed mode bifurcates supercritically at $F^2 = \mu^2+\Omega^2$ when $(p+q+r)\Omega > 0$, and that the bifurcation is subcritical when $(p+q+r)\Omega < 0$.

3.3.2. *Case when sin* $2(\phi-\psi) \neq 0$: *general mode*

Another type of solution occurs when $\sin 2(\phi-\psi) \neq 0$. From (3.22*a*, *b*, *c*, *d*) we get

$$a^2-b^2 = \frac{2\mu}{p-q-r}\frac{\cos 2(\phi-\psi)-1}{\sin 2(\phi-\psi)} \quad \text{and} \quad a^2+b^2+-\frac{2\Omega}{p+q-r}, \tag{3.27a, b}$$

with

$$\cos^2(\phi-\psi) = (4r(p-q+r)\mu^2+(p-q-r)^2F^2 \pm D^{\frac{1}{2}})\Big/\left[8r^2\left\{\mu^2+\frac{(p-q-r)^2}{(p+q-r)^2}\Omega^2\right\}\right] \tag{3.27c}$$

$$D = (p-q-r)^4F^4+8r(p-q+r)(p-q-r)^2\mu^2F^2-16r^2\frac{(p-q+r)^2}{(p+q-r)^2}(p-q-r)^2\mu^2\Omega^2. \tag{3.27d}$$

Because $a^2 \neq b^2$ and $ab \neq 0$, we call this solution the general mode. From (3.27*b*), the general mode exists only when Ω and $p+q-r$ have different signs.

Since $|a^2-b^2| \leqslant |a^2+b^2|$,

$$\cos^2(\phi-\psi) \geqslant \mu^2\Big/\left\{\mu^2+\frac{(p-q-r)^2}{(p+q-r)^2}\Omega^2\right\}. \tag{3.28}$$

Therefore, we have to consider (3.28) together with $\cos^2(\phi-\psi) \leqslant 1$. Without a loss of generality, we can suppose that $a^2 \geqslant b^2$. Knowing that

$$a^2 = \pm\frac{\mu}{p-q-r}\left[\frac{1-\cos^2(\phi-\psi)}{\cos^2(\phi-\psi)}\right]^{\frac{1}{2}}-\frac{\Omega}{p+q-r}, \tag{3.29}$$

which is obtained by eliminating b^2 from (3.27*a*, *b*), does not exist at $F^2 \ll 1$ because $D < 0$, that $a^2 \to \infty$ as $F^2 \to \infty$, and that a^2 is symmetric with respect to $a^2 = -\Omega/(p+q-r)$, we can draw possible pictures of a^2 against F^2 (see figure 4). a^2 is four-valued at most. Turning points can occur at $\cos^2(\phi-\psi) = 1$ and at $D = 0$. It is interesting to see that $\cos^2(\phi-\psi) = 1$ takes place at

$$F^2 = \mu^2+\frac{4r^2}{(p+q-r)^2}\Omega^2 \equiv R_2, \quad a^2 = -\frac{\Omega}{(p+q-r)}, \quad (= b^2)$$

and that the equality in (3.28)

$$\cos^2(\phi-\psi) = \mu^2\Big/\left\{\mu^2+\frac{(p-q-r)^2}{(p+q-r)^2}\Omega^2\right\}$$

holds at $F^2 = R_1$, where $a^2 = -2\Omega/(p+q-r)$ and $b^2 = 0$. Between these points $\cos^2(\phi-\psi)$ changes monotonically. Since we suppose that $a^2 \geqslant b^2$, a^2 can take values only between $-\Omega/(p+q-r)$ and $-2\Omega/(p+q-r)$. The segment of a^2 between 0 and $-\Omega/(p+q-r)$ in figure 4 can be regarded as the graph of b^2.

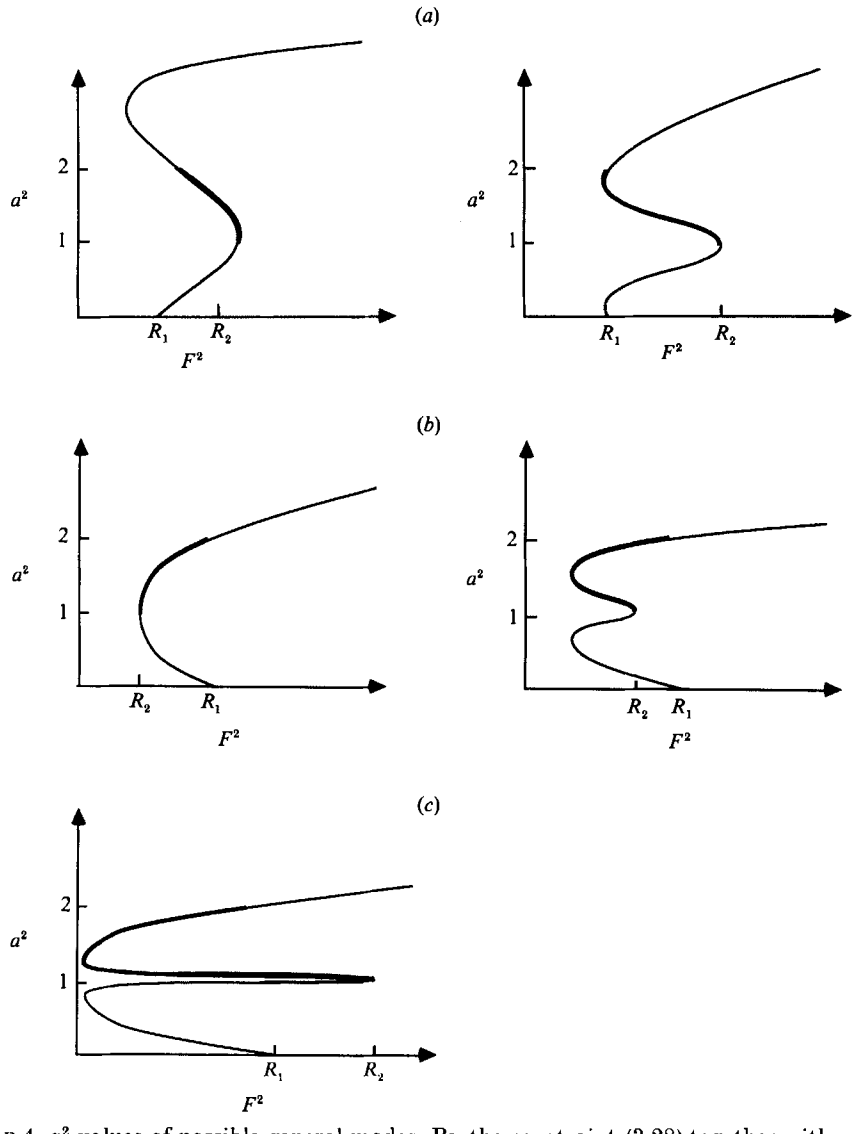

FIGURE 4. a^2 values of possible general modes. By the constraint (3.28) together with $\cos 2(\phi-\psi) \leqslant 1$, general modes can exist only on a segment indicated by a thick curve. a^2 is normalized by $\Omega/(-p-q+r)$. Only the case with $a^2 \geqslant b^2$ is shown. (*a*) $R_2 > R_1$, (*b*) $R_1 > R_2$, (*c*) $0 < \mu \ll 1$.

It may be instructive to describe the behaviour of a^2 when μ is small. From the expression for the general mode solution (3.29) with (3.27*c*, *d*), we get easily

$$a^2 \approx -\frac{\Omega}{p+q-r} \quad (F^2 \leqslant R_2) \quad \text{and} \quad a^2 \approx \pm\frac{F}{p-q+r} - \frac{\Omega}{p+q-r} \quad (F^2 \leqslant R_1)$$

for $F^2 \gg \mu$. The turning points occur at

$$F^2 = \frac{4r|p-q+r|}{(p+q-r)(p-q-r)}\mu\Omega.$$

This situation is illustrated in figure 4(*c*).

3.3.3. *Stability of mixed modes*

Now, local stability properties of the mixed mode ($a^2 = b^2$) solutions are examined. Perturbations $\tilde{A}$ and $\tilde{B}$ superimposed on the x-wave A and y-wave B, respectively, satisfy

$$\mathrm{i}\left(\frac{\partial}{\partial T}+\mu\right)\tilde{A} = \Omega\tilde{A}+F\tilde{A}+p(A^2\tilde{A}^*+2|A|^2\tilde{A}) \\ +q(|B|^2\tilde{A}+AB^*\tilde{B}+AB\tilde{B}^*)+r(B^2\tilde{A}^*+2A^*B\tilde{B}), \quad (3.30a)$$

$$\mathrm{i}\left(\frac{\partial}{\partial T}+\mu\right)\tilde{B} = \Omega\tilde{B}+F\tilde{B}^*+p(B^2\tilde{B}^*+2|B|^2\tilde{B}) \\ +q(|A|^2\tilde{B}+A^*B\tilde{A}+AB\tilde{A}^*)+r(A^2\tilde{B}^*+2AB^*\tilde{A}). \quad (3.30b)$$

Since

$$\mathrm{e}^{\pm\mathrm{i}(\phi-\psi)} = \begin{cases} 1 & (N\text{even}) \\ -1 & N\text{odd}), \end{cases} \quad (3.31a)$$

$$\mathrm{e}^{\mathrm{i}(\phi+\psi)} = \begin{cases} \mathrm{e}^{2\mathrm{i}\phi} & (N\text{even}) \\ -\mathrm{e}^{2\mathrm{i}\phi} & (N\text{odd}) \end{cases} \quad (3.31b)$$

and

$$\mathrm{e}^{2\mathrm{i}\phi} = \mathrm{e}^{2\mathrm{i}\psi} \quad (\text{always}) \quad (3.31c)$$

for $\sin^2(\phi-\psi) = 0$ or $\phi = \psi+N\pi$ (N even or odd), it is found that (3.30a, b) can be reduced to

$$\mathrm{i}\left(\frac{\partial}{\partial T}+\mu\right)\tilde{\chi} = \Omega\tilde{\chi}+F\tilde{\chi}^*+(p+q+r)\,a^2(\mathrm{e}^{2\mathrm{i}\phi}\tilde{\chi}^*+2\tilde{\chi}) \quad (3.32a)$$

and

$$\mathrm{i}\left(\frac{\partial}{\partial T}+\mu\right)\tilde{\rho} = \Omega\tilde{\rho}+F\tilde{\rho}^*+pa^2(\mathrm{e}^{2\mathrm{i}\phi}\tilde{\rho}^*+2\tilde{\rho})-qa^2\,\mathrm{e}^{2\mathrm{i}\phi}\tilde{\rho}^*+ra^2(\mathrm{e}^{2\mathrm{i}\phi}\tilde{\rho}^*-2\tilde{\rho}) \quad (3.32b)$$

for

$$\tilde{\chi} = \tilde{A}+\tilde{B}, \quad \tilde{\rho} \equiv \tilde{A}-\tilde{B} \quad (3.33a)$$

when N is even, and for

$$\tilde{\chi} = \tilde{A}-\tilde{B}, \quad \tilde{\rho} = \tilde{A}+\tilde{B} \quad (3.33b)$$

when N is odd.

Since

$$(p+q+r)\,a^2 = pa_0^2 \quad (3.34a)$$

and

$$\phi = \theta \quad (3.34b)$$

by (3.5a, b) and (3.26a, b), equation (3.32a) is identical to (3.6a), so that the stability properties of the single mode with respect to $\tilde{A}$, which we have explored in the previous subsection, hold for the eigenvalue problem associated with (3.32a). Therefore, we have only to analyse (3.32b). The transformation procedure described above reduces the cumbersomeness which prevented Feng & Sethna (1989) from solving (3.30a, b) analytically when the symmetry-breaking parameter is present.

After some manipulation, we find that the eigenvalue λ with $\rho \propto \mathrm{e}^{\lambda T}$ for (3.32*b*) satisfies

$$(\lambda+\mu)^2 = \left\{\frac{(3p-q-r)(-p-q+3r)}{(p+q+r)^2} - 1 + \frac{4(p-r)}{p+q+r}\right\}\Omega^2$$
$$+\left\{\frac{(3p-q-r)(-p-q+3r)}{(p+q+r)^2} + 1 - \frac{2(p-q+r)}{p+q+r}\right\}F^2$$
$$+\left\{-\frac{(3p-q-r)(-p-q+3r)}{(p+q+r)^2} + \frac{2(p-q+r)}{p+q+r}\right\}\mu^2$$
$$\pm 2\left\{-\frac{(3p-q-r)}{(p+q+r)^2} - \frac{p+q-3r}{p+q+r}\right\}\Omega(F^2-\mu^2)^{\frac{1}{2}}, \tag{3.35}$$

where the double sign $\pm$ is consistent with that of the expression for a or b in (3.26*a*). The method to determine whether the right-hand side is larger or smaller than μ^2 at given F^2 with fixed Ω is basically the same as described in §3.1. Therefore, we just describe results which are derived from (3.35) in the following.

For the supercritical branch with $p+q+r<0$ and $\Omega<0$, the mixed mode is unstable only when $p+q-r<0$, $p+q-3r>0$ and $F^2>R_2$, whereas the mixed mode on the supercritical branch with $p+q+r>0$ and $\Omega>0$, is stable only when $p+q-r<0$, $p+q-3r<0$ and $F^2>R_2$. For the subcritical solutions, when $p+q-r>0$, the lower branch is stable and the upper branch is unstable for $F^2>R_2$, irrespective of the sign of $p+q+r$. When $p+q-r<0$, although the upper branch is stable for both $p+q+r>0$ and $p+q+r<0$, the lower branch is unstable for $R_2<F^2<\mu^2+\Omega^2$ only if $p+q+r<0$. Since $p+q-r<0$ and $r>0$ always, $p+q-3r$ is negative. This eliminates many possibilities. This statement must be combined with the normal stability property derived from (3.32*a*) in order to make stability analysis for the mixed mode complete.

All the realizable bifurcation pictures are classified in figure 5 in terms of αh. When $\Omega<0$, the mixed mode is always preferred. The general mode exists only when $\Omega>0$. The general mode connects two points at $F^2=R_1$ on the single mode branch and at $F^2=R_2$ on the mixed mode branch where one of the four eigenvalues changes sign. The general mode may be double-valued, as indicated in figure 4. It can be proved that the turning point of the general mode, if it exists, does not occur at F^2 smaller than μ^2. The case in figure 5(*a*) corresponds to the one analysed by Feng & Sethna (1989). They considered the case more generally by introducing a slight difference between the two side lengths of the base. But we believe that there are some points yet to be made clear in their analysis. For instance, in their figure 2 the behaviour of the single modes OM2 and OM4 and the mixed mode MS2 at small forcing amplitude (corresponding to their large $|\sigma|$ with $\sigma<0$) is not clear, whereas the $\Omega<0$ part of our figure 5(*a*) shows that the subcritical branches for both single and mixed modes have turning points at $F^2=\mu^2$. The stability of the general mode will be analysed numerically in the next section for a few selected cases.

4. Numerical examples

In this section, finite-amplitude standing wave motions and their stability are examined numerically following Nagata *et al.* (1989). For the finite-amplitude solutions, a Newton–Raphson method is used whereas we use a matrix inversion method to solve eigenvalue problems. Also, trajectories in the four-dimensional space

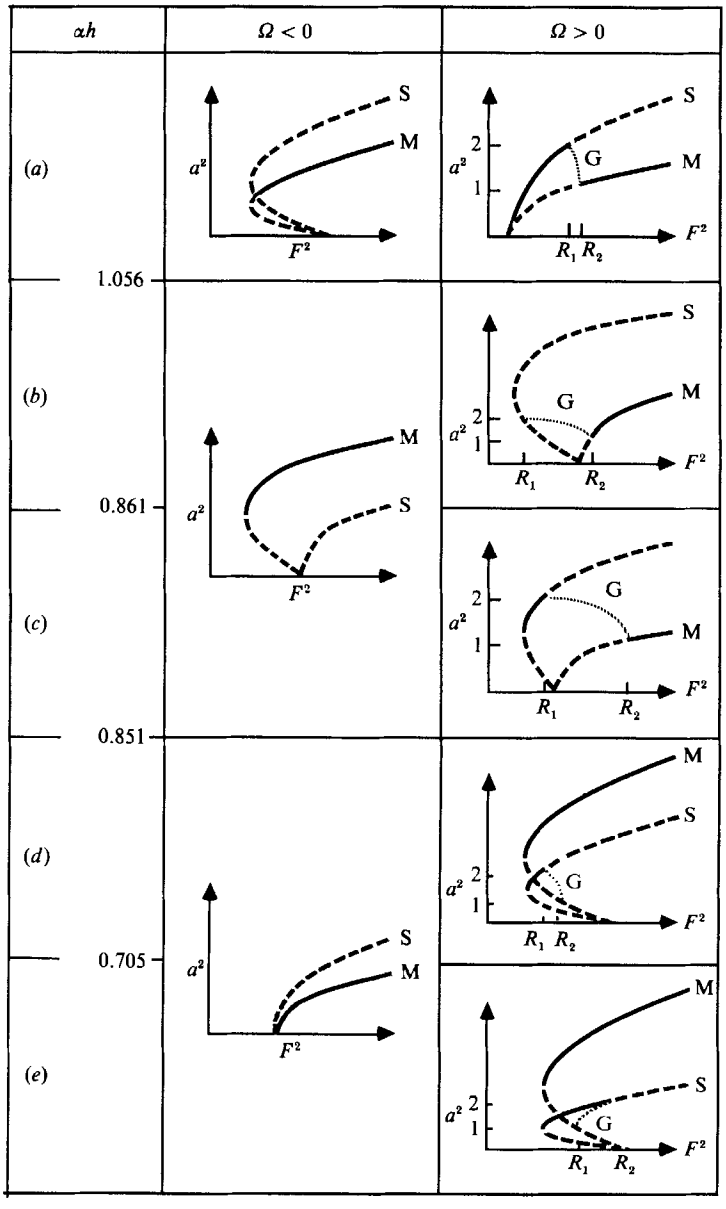

FIGURE 5. Bifurcation diagram. The single surface mode and the mixed surface mode are represented by letters S and M, respectively. Stable branches are indicated by a full curve whereas unstable branches are indicated by a dashed curve. For the general mode indicated by a letter G and by a dotted curve, stability has not been examined anayltically. a^2 is normalized by $\Omega/(-p-q+r)$.

of A_R, A_I, B_R, B_I representing real and imaginary parts of both A and B are followed with respect to time T from given initial values in order to see how stable standing wave motions attract, especially when stable solutions are not unique. Of course from the symmetry of the system, if (A_R, A_I, B_R, B_I) is a solution, then $(A_R, A_I, -B_R, -B_I)$, $(-A_R, -A_I, B_R, B_I)$, $(-A_R, -A_I, -B_R, -B_I)$ and the ones with A and B interchanged are also the solutions in general. But we are more interested in

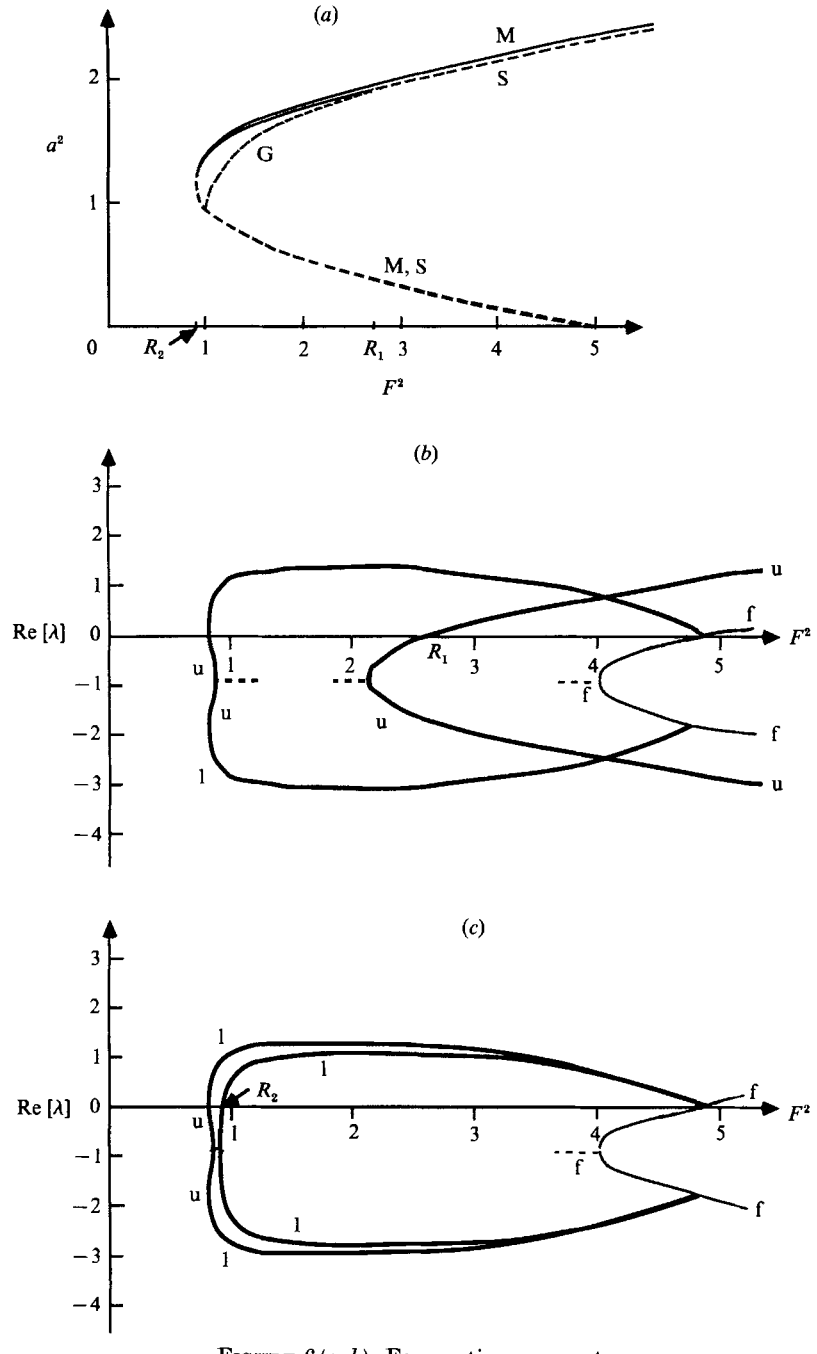

FIGURE 6(*a–b*). For caption see next page.

situations where additional modes of wave motions coexist. The set of evolution equations (2.14*a*, *b*) is integrated with a fourth-order Runge–Kutta algorithm.

We select the case with $\sigma = 0.5$, $\mu = 0.9$ and $\Omega = 2.0$, corresponding to the $\Omega > 0$ part of figure 5(*e*). This case is particularly interesting because there exists a 'window' in the subcritical parameter region where three different stable modes coexist: namely, flat surface, single surface wave and mixed surface wave. Although

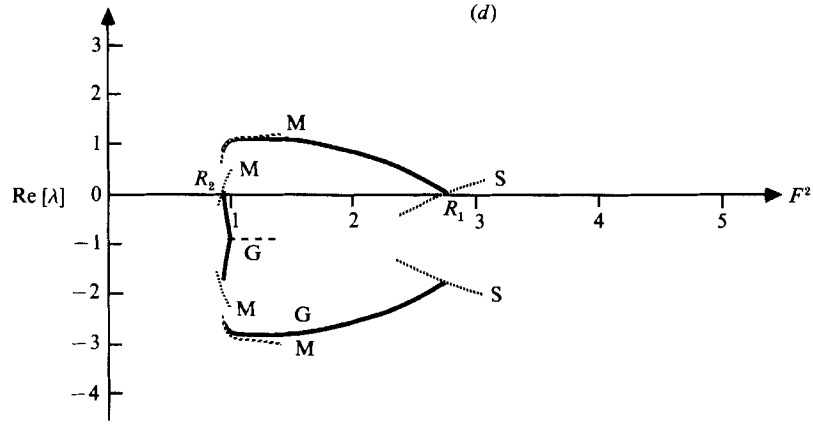

FIGURE 6. Case with $\sigma = 0.5$, $\mu = 0.9$, $\Omega = 2.0$ and $\alpha = 1.0$. (*a*) Plot of a^2 normalized by $\Omega/(-p-q+r)$ for various modes as a function of the control parameter F^2. For description, see figure 5. The eigenvalues are shown in (*b*) are for the single mode, (*c*) the mixed mode and (*d*) the general mode. Letters l and u indicate a lower branch and an upper branch, respectively. The eigenvalues for the flat surface indicated by a letter f are also shown in (*b*) and (*c*). Some portions of (*b*) and (*c*) are duplicated in (*d*).

Feng & Sethna (1989) claim that physically wave motions are inhibited when $\alpha h < 1.0$ owing to a strong damping effect, the case sets in at $\alpha h = 0.705$, which is well within the possible range of experiments.

The single mode and the mixed mode bifurcate subcritically at $F^2 = 4.81$. The turning points of both modes occur at the common value of $F^2 = \mu^2 = 0.81$. The general mode, which connects a point on the lower mixed mode branch at $F^2 = R_2 = 0.918379$ and a point on the upper single mode branch at $F^2 = R_1 = 2.72420$ without a turning point, is found to be always unstable. The mixed mode is stable for $F^2 > \mu^2$, whereas the single mode is stable only for $\mu^2 < F^2 < R_1$ (see figure 6). The parameter region $\mu^2 < F^2 < R_1$, where both single and mixed modes together with the flat surface are stable, has been investigated numerically for many different critical states. The final point to which trajectories are attracted depends on these initial values as shown in figure 7. For instance, when initial values with $A_I = B_I = 0$ are chosen, trajectories starting on or near the line $B_R = 0$ in (A_R, B_R)-space are attracted to one of the two single modes with $B = 0$ or to the origin, whereas trajectories starting on or near the line $B_R = A_R$ are attracted to one of the two mixed modes with $A = B$ or to the origin. Between these two lines, all possible forms of stable solution can be reached. For initial values with $B_R = 0$ together with $A_I = B_I = 0$, the trajectories remain on the manifold of $B = 0$ at all times. Figure 7(*a*) is such an example. This intertwined structure was analysed theoretically by Gu, Sethna & Narain (1987) when they dealt with one mode dynamics, and evidence of such a structure was observed experimentally by Simonelli & Gollub (1989). In our three-dimensional problem, a similar intertwined structure of trajectories can also be seen on the invariant manifold $A = B$ (see figure 7*b*) when initial values satisfy $A = B$. Phase space trajectories are much more complicated for initial values $A_R \neq B_R \neq 0$ (figure 7*c*) than for the two extreme cases just described.

Two other interesting cases emerge from figures 5(*b*) and 5(*d*) when $\Omega > 0$. The stability arguments described in §3.2 for the single mode and in §3.3.3 for the mixed mode indicate, with the aid of the principle of exchange of stability, that the general mode in both cases has two positive real eigenvalues near one of the bifurcation

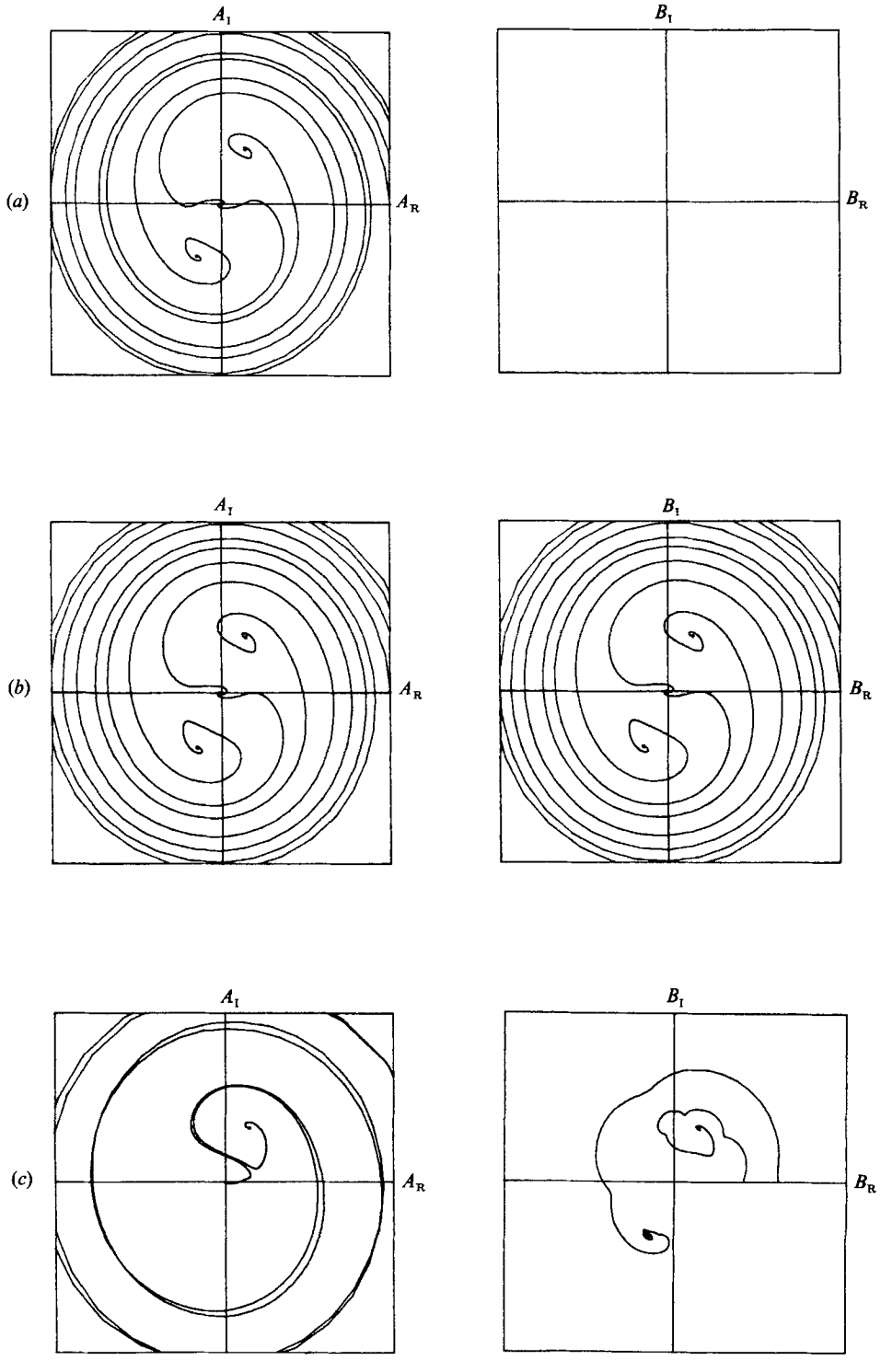

FIGURE 7. Projection of trajectories on the phase planes (A_R, A_I) and (B_R, B_I). Trajectories are attracted to: (*a*) flat surface or single modes when $c_2 = 0$, (*b*) the flat surface or mixed mode when $c_1 = c_2$, (*c*) the single mode or the mixed mode when $c_1 \neq c_2$, where $c_1 \geqslant 0$ and $c_2 \geqslant 0$ are initial values of A_R and B_R, i.e. $(A_R(0), A_I(0), B_R(0), B_I(0)) = (c_1, 0, c_2, 0)$.

points at $F^2 = R_1$ or $F^2 = R_2$ and two negative real eigenvalues near the other bifurcation point. Therefore, either the two eigenvalues change signs individually somewhere between the bifurcation points, or a Hopf bifurcation occurs from the general mode. The latter turns out to be the case. Numerical calculations for $\sigma = 0.75$, $\mu = 1.0$ and $\Omega = 2.0$ reveal two negative eigenvalues, one of which is zero at $F^2 = R_2$, merging together to transform themselves into a complex conjugate pair with negative real part as F^2 is decreased from $F^2 = R_2 \approx 11.79$. Then, this pair crosses the imaginary axis on the complex plane at $F^2 = 10.2$ before it is separated into two positive eigenvalues towards $F^2 = R_1 = 2.09$.

The whole sequence occurs in the reverse order in the case with $\sigma = 0.65$, $\mu = 1.0$ and $\Omega = 2.0$, which corresponds to figure 5(*d*).

The structure of this time-dependent solution, especially in the first case, seems to be very rich; periodic and heteroclinic orbits and chaotic behaviour have been observed in a provisional analysis. More detailed investigations are underway.

5. Conclusion

Competition between single and mixed surface wave motions has been investigated in a container with a square base. The results obtained analytically are classified in figure 5 according to coefficients p, q and r of the nonlinear terms of the coupled evolution equations. These coefficients are determined explicitly by αh. It is found that in any case the mixed mode is preferred when $\omega < \omega_0$ and the general mode solution exists only when $\omega > \omega_0$. Numerical calculations were carried out, in particular to analyse the stability of the general mode. Also, by integrating the coupled evolution equations numerically, complicated ways of how multiple stable fixed points attract trajectories were revealed. Intertwined structures of trajectories were observed in the four-dimensional phase space by imposing specific initial conditions $B_R = 0$ or $A_R = B_R$ with $A_I = B_I = 0$ when a stable single mode and a stable mixed mode coexist. For initial conditions with $A_R \neq B_R \neq 0$ with $A_I = B_I = 0$, typical sizes of the basins of attraction for each fixed point become smaller as the distance of initial values from the origin increases (see figure 8). There are nine attractors and the basins in the four-dimensional phase space are entangled in a complicated way. Complicated structures of the basins of multiple coexisting attractors are reported in other systems (Battelino *et al.* 1988).

The Hopf bifurcations are detected on the general mode branch in §4 for some parameter values. Successive bifurcations from the periodic solution leading to chaos will be discussed in a separate paper shortly.

For the special value of σ for which $p = 0$ or $p+q+r = 0$ etc, the problem becomes degenerate and higher-order terms must be taken into account.

After this work was presented at Euromech 236 (Cambridge, 1988), the author received a preprint of Feng & Sethna (1989). Their simultaneous research was drawn to the author's attention by Professor J. P. Gollub, to whom the author is greatly indebted. Also, the author would like to thank Professor A. D. D. Craik for giving him an opportunity to work under grant supported by SERC. Discussion with him is greatly appreciated.

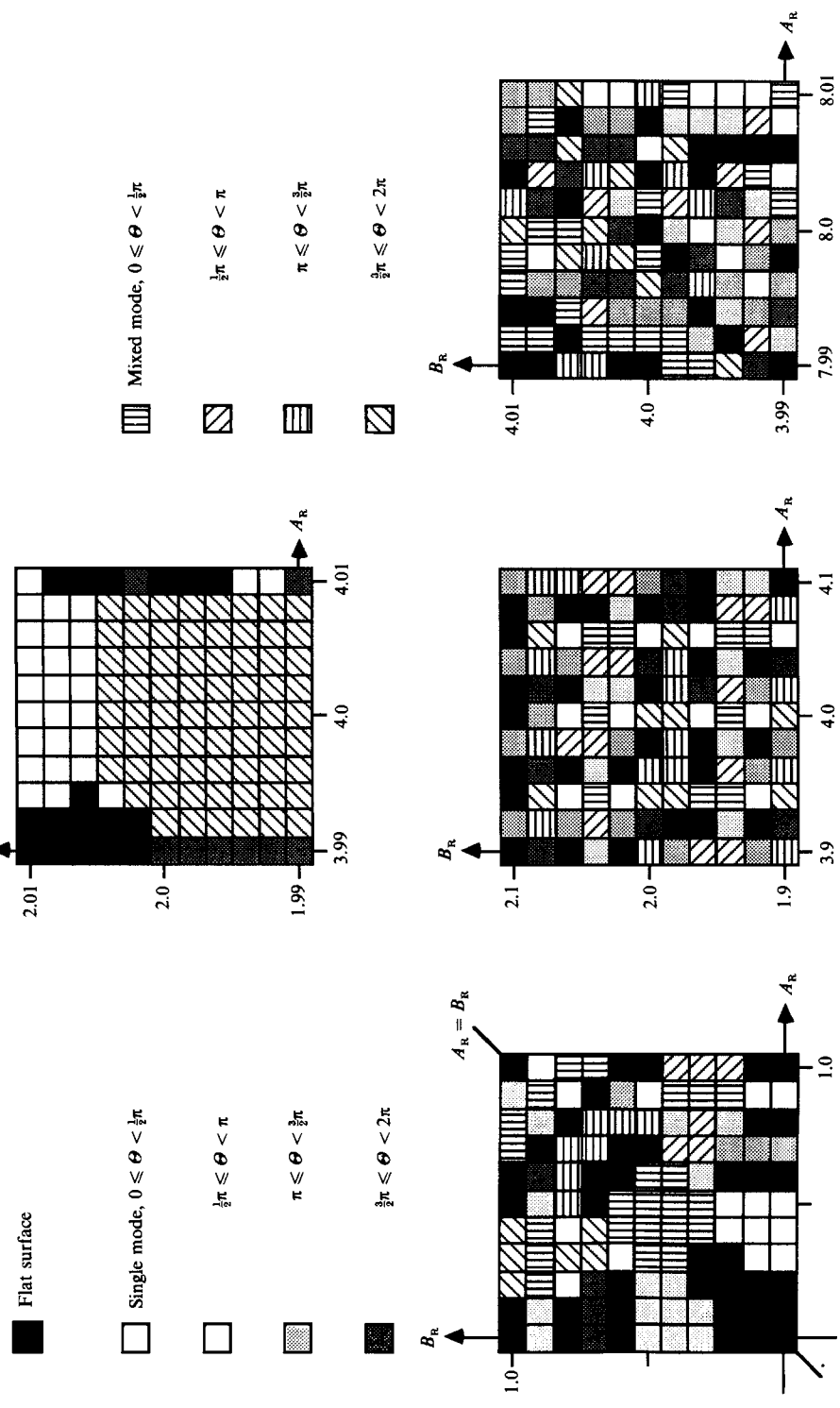

FIGURE 8. The basins of attraction of the various fixed points. Initial values with $A_R \geqslant 0$, $A_I = 0$, $B_R \geqslant 0$, $B_I = 0$ are chosen. Various patterns indicate both the mode and the quadrant of the $(A_R(\infty), B_R(\infty))$-plane to which trajectories are attracted. $\theta = \arctan(B_R(\infty)/A_R(\infty))$.

REFERENCES

BATTELINO, P. M., GREBOGI, C., OTT, E., YORKE, J. A. & YORKE, E. D. 1988 Multiple coexisting attractors, basin boundaries and basic sets. *Physica* D **32**, 296–305.

BENJAMIN, T. B. & URSELL, F. 1954 The stability of the plane free surface of a liquid in vertical periodic motion. *Proc. R. Soc. Lond.* A **225**, 505–517.

CILIBERTO, S. & GOLLUB, J. P. 1984 Pattern competition leads to chaos. *Phys. Rev. Lett.* **52**, 922–925.

CILIBERTO, S. & GOLLUB, J. P. 1985 Chaotic mode competition in parametrically forced surface waves. *J. Fluid Mech.* **158**, 381–398.

DRAZIN, P. G. & REID, W. H. 1981 *Hydrodynamic Stability*. Cambridge University Press.

FARADAY, M. 1831 On the forms and states assumed by fluids in contact with vibrating elastic surfaces. *Phil. Trans. R. Soc. Lond.* **121**, 319–346.

FENG, Z. C. & SETHNA, P. R. 1989 Symmetry-breaking bifurcations in resonant surface waves. *J. Fluid Mech.* **199**, 495–518.

GOLLUB, J. P. & MEYER, C. W. 1983 Symmetry-breaking instabilities on a fluid surface. *Physica* D **6**, 337–346.

GU, X. M., SETHNA, P. R. & NARAIN, A. 1987 On three-dimensional nonlinear subharmonic resonant surface waves in a fluid. Part I. Theory. *Trans. ASME* E: *J. Appl. Mech.* **55**, 213–219.

HOLMES, P. J. 1986 Chaotic motions in a weakly nonlinear model for surface waves. *J. Fluid Mech.* **162**, 365–388.

JENKINS, D. R. 1987 Rolls versus squares in thermal convection of fluids with temperature-dependent viscosity. *J. Fluid Mech.* **178**, 491–506.

KEOLIAN, R., TURKEVICH, L. A., PUTTERMAN, S. J., RUDNICK, I. & RUDNICK, J. A. 1981 Subharmonic sequences in the Faraday experiment: departures from period doubling. *Phys. Rev. Lett.* **47**, 1133–1136.

LARRAZA, A. & PUTTERMAN, S. 1984 Theory of non-propagating surface-wave solitons. *J. Fluid Mech.* **148**, 443–449.

MERON, E. 1987 Parametric excitation of multimode dissipative systems. *Phys. Rev.* A **35**, 4892–4895.

MILES, J. W. 1984*a* Nonlinear Faraday resonance. *J. Fluid Mech.* **146**, 285–302.

MILES, J. W. 1984*b* Parametrically excited solitary waves. *J. Fluid Mech.* **148**, 451–460.

NAGATA, M., PROCTOR, M. R. E. & WEISS, N. O. 1989 Transitions to asymmetry in magnetoconvection. *Geophys. Astrophys. Fluid Dyn.* (to appear).

RAYLEIGH, LORD 1883*a* On maintained vibrations. *Phil. Mag.* **15**, 229–235 (Scientific Papers, Vol. 2, pp. 188–193),

RAYLEIGH, LORD 1883*b* On the crispations of fluid resting on a vibrating support. *Phil. Mag.* **16**, 50–58 (Scientific Papers, Vol. 2, pp. 212–219).

SIMONELLI, F. & GOLLUB, J. P. 1989 Surface wave mode interactions: Effects of symmetry and degeneracy. *J. Fluid Mech.* **199**, 471–494.

SWIFT, J. W. 1984 Bifurcation and symmetry in convection. Ph.D. dissertation, University of California, Berkeley.

WU, J., KEOLIAN, R. & RUDNICK, I. 1984 Observation of a non-propagating hydrodynamic soliton. *Phys. Rev. Lett.* **52**, 1421–1424.